STUDIES

Surface curvature analysis of bivariate normal distribution: A Covid-19 data application on Turkey

Vahide Bulut
Department of Engineering Sciences,
Izmir Katip Celebi University, Turkey
E-mail: vahide.bulut@ikcu.edu.tr

Serdar Korukoglu
Department of Computer Engineering,
Ege University, Turkey
E-mail: serdar.korukoglu@ege.edu.tr

Principal curvatures have free-form rigid surfaces' invariant features. Therefore they are widely used in several fields for various applications, such as determining the corresponding points between an object and a free-form scene. In this study, the authors analysed the surface curvature of a bivariate normal distribution. A novel approach for classifying bivariate normal surfaces based on curvature statistics concerning correlation structures is presented. The principal curvatures, Gaussian, and mean curvatures were obtained using the data generated from the bivariate normal distribution. The degree of dependency bivariate data directly affects the shape and curvature structures of the bivariate normal distribution surface. Different parameters, from uncorrelated to highly correlated variables, for the correlation of the bivariate normal distribution based on the data have been examined. The effects of the correlation on the distribution surface characteristics have been analysed individually and collectively. This study presents theoretical results in addition to the results of the simulation and real datasets. The simulation data presents the relationship between the independence of the variables and the uniformity of the κ_{n2} values. The other application is based on the curvature properties of the bivariate normal surface on Covid-19 as real data.

Keywords:
principal curvatures,
Gaussian curvature,
mean curvature,
bivariate normal distribution,
correlation

Introduction and literature review

Principal curvatures, principal directions, and normals are used in 3D computer vision to solve basic tasks, such as segmentation, surface classification, surface reconstruction, and registration Krsek et al. (1998). Since the principal curvatures at a surface point are invariant properties, these curvatures are used for surface characterisation. Researchers have studied many methods to estimate the Gaussian and mean curvatures on various surfaces such as faces and human bodies. In Tanaka et al. (1998), the authors presented a correlation-based face recognition approach based on the analysis of principal curvatures. The authors Vemuri et al. (1986) used principal curvatures for shape recognition from range data, while in Deng et al. (2007), the authors used these curvatures for object recognition. In Bedi et al. (1997), two methods for machining complex three-dimensional surfaces on 4 and 5 axis machines are proposed to align the principal axis of the curvature of the machining surface with that of the machined surface to increase the volume of the removed material. Authors Floro–Chason (2001) studied the use of a curvature technique called a multi-beam optical stress sensor. In Sboui et al. (2017), the authors proposed a local surface description around the 3D human body extremities based on the mean of the principal curvature field values on the intrinsic Darcyan parameterisation. Justin et al. (Lev et al. (2017)) presented a new local measure based on the principal curvatures of a point cloud for 3D shape recognition. In Tremblay-Darveau et al. (2018), the authors showed that the principal curvature detection could significantly improve the 3D rendering of relatively noisy ultrasound angiograms without degrading the spatial resolution. Moreover, the authors Wang et al. (2018) proposed a shape- similarity measurement approach based on principal curvatures.

The normal distribution of statistics has great importance in different fields such as economics, medicine, actuarial sciences, and engineering. Azzalini (1985) studied the standard normal-density function and its properties. In Azzalini–Chiogna (2004), the authors gave some exact probability results on the stress–strength model in the case of skew-normal variates. Henze (1986) presented a probabilistic representation of the skew-normal distribution in the normal and truncated normal law. In Branco–Dey (2001), the authors proposed a new class of multivariate skew-elliptical distributions, which bring additional flexibility of modeling skewed data. A class of multivariate unified skew-elliptical distributions is presented in Arellano-Valle–Genton (2010). The authors proposed a new model distribution, known as the bivariate Weibull-Geometric distribution in Kundu–Gupta (2014). In Roozegar–Jafari (2017), the authors expressed the bivariate generalized linear failure rate-power series model as a new class of bivariate distributions. The authors studied a new bivariate distribution and its distributional properties with normal geometric distribution marginal in Mahmoudi–Mahmoodian (2017). In Omair et al. (2018), the authors introduced a new bivariate model and its distributional properties combining negative binomial and geometric distributions. In Jafari et al. (2018), the authors expressed a new model for bivariate distribution and provided different properties of this distribution by combining the bivariate generalized exponential and power-series distributions. The authors studied a method based on particle swarm optimisation and bivariate normal inverse Gaussian distribution to comprehensively understand the joint period and radius distribution in Kepler exoplanets in Chen–Hung (2019). Additionally, in Jamalizadeh–Balakrishnan (2019), the conditional distribution of a Multivariate Normal Mean-Variance Mixture (MNMVM) distribution is expressed. Shimamoto (2019) examined Japan according to urban park area per capita. The vagueness in the shape-from-shading inference problem is examined in Holtmann-Rice et al. (2018). The author studied the multivariate normal model from the Riemannian geometry perspective by accepting the model as a differentiable manifold in Theil (1984). Colour raster graphics and differential geometry are merged to analyse the surface curvature in Dill (1981).

This study examines the bivariate normal distribution by combining the principal curvatures, Gaussian, and mean curvatures. Additionally, some results based on the relationships between the bivariate normal distribution and surface curvatures are given. Our purpose is to present how to utilise the principal curvatures to examine the characteristic similarities and differences of two normal distributed bivariate real data. This provides a better understanding of real data besides statistical analyses. This study desires to use geometry for statistical inference as a bivariate normal distribution and Covid-19 outbreak.

The remainder of this paper is organised as follows. Preliminary theoretical information about the curvatures of a surface and bivariate normal distribution are briefly reviewed. The surface analysis of the bivariate Gaussian distribution, including the experiments, is presented. Two applications are given to present the relationship between the independence of the variables and the curvature properties of the bivariate normal surface on Covid-19 data. Finally, the paper presents the conclusions.

Theoretical foundations

This section briefly describes the curvatures of a surface and the bivariate normal distribution.

Principal curvatures of a surface

A surface that is a piece of $\mathbb{R}^2$ in the vicinity of any given point is a subset of $\mathbb{R}^3$.

Definition 1: A surface patch $\mathbf{D}: U \to \mathbb{R}^3$ is called regular if it is smooth and the vectors $\mathbf{D_u}$ and $\mathbf{D_v}$ are linearly independent at all points $(u, v) \in U$.

A unit normal of the surface $\mathbf{S}$ at a point $\mathbf{p}$ can be defined with

$$\mathbf{n_D} = \frac{\mathbf{D_u} \times \mathbf{D}_v}{\|\mathbf{D_u} \times \mathbf{D}_v\|}.$$

Definition 2: Let $\mathbf{D}(u, v)$ be a surface patch of $\mathbf{S}$ and $\boldsymbol{\alpha}(t) = \mathbf{D}(u(t), v(t))$ be a unit speed curve in $\mathbf{D}$. The normal curvature of the curve is obtained using

$$\kappa_n = L\dot{u}^2 + 2M\dot{u}\dot{v} + N\dot{v}^2,$$

in which L, M and N are coefficients of the second fundamental form defined as

$$L = \mathbf{D_{uu}n}, \quad M = \mathbf{D_{uv}}.\mathbf{n}, \; and \quad N = \mathbf{D_{vv}}.\mathbf{n}.$$

Proposition: Let $\mathbf{p}$ be the point of surface $\mathbf{S}$. The principal curvatures, κ_{n1} and κ_{n2} are scalar values, and they are the maximum and minimum of the normal curvature, respectively, at point $\mathbf{p}$ on surface $\mathbf{S}$. The principal curvatures are related to the mean and Gaussian curvatures in a simple manner, with

$$K = \kappa_{n1}.\kappa_{n2} \; and \quad H = \frac{\kappa_{n1} + \kappa_{n2}}{2}.$$

The principal curvatures can be written in terms of the Gaussian and normal curvatures by

$$\begin{cases} \kappa_{n1} = H + \sqrt{H^2 - K} \\ \\ \kappa_{n2} = H - \sqrt{H^2 - K}. \end{cases}$$

The values of the principal and Gaussian curvatures κ_{n1}, κ_{n2} and K play an important role in determining the shape of the surface. At the points of a surface, if $K = \kappa_{n1}.\kappa_{n2} > 0$, then these points are elliptical; if $K = \kappa_{n1}.\kappa_{n2} < 0$, then these points are hyperbolic, and if $K = \kappa_{n1}.\kappa_{n2} = 0$, then these points are parabolic Pressley (2010). For an embedded smooth surface in R^3, the Gaussian curvature is invariant under the local isometries. The classification of the points on a surface is presented in Table 1.

Table 1

Classification of points on a surface according to principal curvatures κ_{n1} and κ_{n2}

	$\kappa_{n1} < 0$	$\kappa_{n1} = 0$	$\kappa_{n1} > 0$
$\kappa_{n2} < 0$	Concave ellipsoid	Concave cylinder	Hyperboloid surface
$\kappa_{n2} = 0$	Concave cylinder	Plane	Convex cylinder
$\kappa_{n2} > 0$	Hyperboloid surface	Convex cylinder	Convex ellipsoid

Bivariate normal distribution

A vector-valued random variable $X = [X_1, \ldots, X_p]^T$ is said to have a multivariate normal distribution with a mean vector $\bar{\mu}$ and a covariance matrix $\sum$ if its probability density function is given by

$$\begin{cases} f(\mathbf{x}; \boldsymbol{\mu}, \Sigma) = \\ \\ \dfrac{1}{(2\pi)^{\frac{d}{2}} |\Sigma|^{\frac{1}{2}}} \exp\left\{-\dfrac{1}{2}(\mathbf{x} - \boldsymbol{\mu})^T \Sigma^{-1} (\mathbf{x} - \boldsymbol{\mu})\right\}. \end{cases}$$

In the case of multivariate normal density, the argument of the exponential function, $\left(-\frac{1}{2}(\mathbf{x} - \boldsymbol{\mu})^T \Sigma^{-1} (\mathbf{x} - \boldsymbol{\mu})\right)$ is a quadratic form of the vector variable $\mathbf{x}$. It is known that the covariance matrix Σ is positive definite, for any vector $\mathbf{x} \neq \boldsymbol{\mu}$. If $(\mathbf{x}-\boldsymbol{\mu})^T\Sigma^{-1}(\mathbf{x}-\boldsymbol{\mu}) > 0$ and $\left(-\frac{1}{2}(\mathbf{x}-\boldsymbol{\mu})^T\Sigma^{-1}(\mathbf{x}-\boldsymbol{\mu})\right) < 0$, then the argument of the exponential function is a downward-opening quadratic bowl. In the case of $p = 2$, the bivariate normal density has the form:

$$f(\mathbf{x}; \boldsymbol{\mu}, \Sigma) = \frac{1}{(2\pi\boldsymbol{\sigma_1\sigma_2})(1-\rho)^{\frac{1}{2}}}\exp\left(-\frac{z}{2(1-\rho)^2}\right)$$

where σ is standard deviation, and

$$\mathbf{z} \equiv \frac{(\mathbf{x_1}-\boldsymbol{\mu_1})^2}{\boldsymbol{\sigma_1^2}} - \frac{2\rho(\mathbf{x_1}-\boldsymbol{\mu_1})(\mathbf{x_2}-\boldsymbol{\mu_2})}{\boldsymbol{\sigma_1\sigma_2}} + \frac{(\mathbf{x_2}-\boldsymbol{\mu_2})}{\boldsymbol{\sigma_2^2}}$$

and also

$$\boldsymbol{\rho} \equiv cor(\mathbf{x_1}, \mathbf{x_2}) = \frac{\boldsymbol{\sigma_{1,2}}}{\boldsymbol{\sigma_1\sigma_2}}$$

which is the correlation of $\mathbf{x_1}$ and $\mathbf{x_2}$.

As known, the contours of a bivariate normal distribution are elliptical. Figure A1 in the Appendix illustrates three cases: positive, negative, and zero correlations.

Surface curvature analysis of bivariate Gaussian distribution

The surface analysis of the bivariate Gaussian distribution is examined using the maximum, minimum, Gauss, and mean curvatures. In this study, 10,000 data are generated based on the mean vector and covariance matrix as

$$\boldsymbol{\mu} = \begin{pmatrix}0\\0\end{pmatrix} \; and \; \Sigma = \begin{pmatrix}1 & \rho\\ \rho & 1\end{pmatrix}.$$

Then, the maximum, minimum, Gaussian, and mean curvatures of these data are computed according to the correlation values of 0.0; 0.1; 0.3; 0.5; 0.7; 0.75; 0.80; 0.85; 0.90, and 0.95. Meanwhile, since the same results are obtained for the negative correlation values, only positive correlation values are considered in this study. The classification of points of the Bell-shaped surfaces, which belong to the data produced using different correlation values, is presented in Table 2. Since different values of κ_{n1} corresponding to the values of $\kappa_{n2} = 0$ and $\kappa_{n2} > 0$ are equal to zero, we did not show these values in Table 2.

For all the examined values of $\boldsymbol{\rho}$, κ_{n2} is obtained as negative, whereas κ_{n1} can receive positive and negative values. At all points on the Bell-shaped surface, the change rate of κ_{n1} sign is 40% and 60%, which is not affected by the change in $\boldsymbol{\rho}$. Next, the relationship between the Gaussian curvature and correlation, as well as the mean curvature and correlation, can be seen in Figures A2 and A3 in the Appendix. The locations where κ_{n1} is calculated as positive and negative compared to the regions of the Bell-shaped surface. Additionally, at the centre of and around the distribution, while K and H take positive values, they turn into negative values in the skirts and exhibit a proportionally unchanged appearance with $\boldsymbol{\rho}$. Figures A4 and A5 in the

Appendix show the distribution of κ_{n1} and κ_{n2}, and in the weak correlations, the distribution of κ_{n1} is skewed to the left, while the right skewness changes gradually for strong correlation values. Conversely, the distribution of κ_{n2} tends to be uniform for small correlation values, while it becomes skewed left for high correlation values. The marginal plots of κ_{n1} and κ_{n2} are shown in Figure A6 in the Appendix. The variation between κ_{n1} and κ_{n2} depending on the different values of $\boldsymbol{\rho}$ is shown in Figure A6.

Table 2

Classification of points of the Bell-shaped surfaces according to different correlation values

ρ	$\kappa_{n1} < 0$ & $\kappa_{n2} < 0$ (%)	$\kappa_{n1} > 0$ & $\kappa_{n2} < 0$ (%)	Total
0.00	39.57	60.43	100.00
0.10	39.90	60.10	100.00
0.30	39.65	60.35	100.00
0.50	40.35	59.65	100.00
0.70	39.52	60.48	100.00
0.75	39.35	60.65	100.00
0.80	39.76	60.24	100.00
0.85	40.21	59.79	100.00
0.90	39.26	60.74	100.00
0.95	39.14	60.86	100.00
Total	39.67	60.33	100.00

Figure 1

The change between the principal curvatures κ_{n1} and κ_{n2} for uncorrelated variables

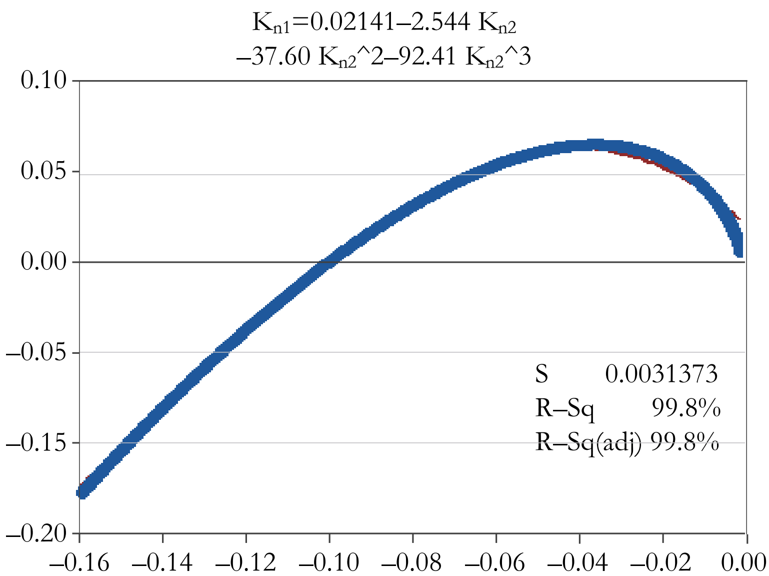

Moreover, in the case of independent variables, the principal curvatures κ_{n1} and κ_{n2} change cubically. The obtained cubic regression polynomial is shown in Figure 1.

As $\boldsymbol{\rho}$ values become greater than zero, the interval changes for both the principal curvatures κ_{n1} and κ_{n2} increase (see Figure 2). Additionally, the average curvature κ_{n2} decreases, whereas the average curvature κ_{n1} increases. Figure 2 shows that the change in κ_{n2} is realised over a wider range. However, it is noteworthy that these changes are not linear.

Figure 2

Interval plots for the principal curvatures κ_{n1} and κ_{n2} according to different values of ρ

95% CI for the mean

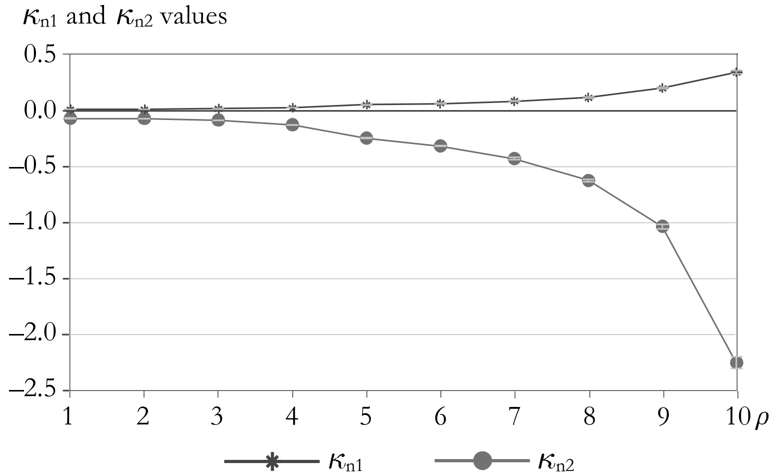

Figure 2 also shows that the principal curvatures κ_{n1} and κ_{n2} change in opposite directions and nonlinearly as the correlation increases. Additionally, it is noteworthy that the principal curvature κ_{n2} changes over a wider range.

Application

In this section we stated that the distribution of κ_{n1} is skewed to the left for small correlations. Simultaneously, it tends to the right for strong correlations, and κ_{n2} tends to be distributed uniformly for small correlations but skewed left for high correlations. Meanwhile, as seen from the graph in Figure A5 in the Appendix, the uniform case for κ_{n2} corresponds to the independence of the normal variables. To show the relationship between the independence of the variables and the uniformity of the κ_{n2} values, we designed two examples.

Example 1

Random samples are generated from the bivariate normal distribution of sizes $n = 50$, $n = 250$, and $n = 1{,}000$ and different correlation values. Pearson's correlation coefficients and 95% confidence intervals are calculated for each sample. Additionally, κ_{n2} values are obtained using the same data. To investigate the distribution of κ_{n2} values, we performed a goodness-of-fit test using Kolmogorov-Smirnov test statistics. The critical region is based on the distribution of the test statistics under the uniformity assumption is true. The results are summarised in Table 3.

Table 3

Pearson's correlation coefficients, 95% confidence intervals and Kolmogorov-Smirnov test results of κ_{n2} values

Value	Correlation			Kolmogorov-Smirnov test		
	r	95%CI		Value	Result	
				n=50		
ro=0,0	–0.158	–0.418	0.126	0.071	Accept	p>0.05
ro=0,1	–0.048	–0.322	0.234	0.06774	Accept	p>0.05
ro=0,3	0.146	–0.138	0.408	0.15346	Accept	p>0.05
ro=0,5	0.569	0.345	0.731	0.09678	Accept	p>0.05
ro=0,7	0.821	0.703	0.895	0.15594	Accept	p>0.05
ro=0,75	0.742	0.584	0.846	0.15951	Accept	p>0.05
ro=0,80	0.824	0.708	0.897	0.13529	Accept	p>0.05
ro=0,85	0.846	0.743	0.91	0.18379	Accept	p>0.05
ro=0,90	0.897	0.825	0.941	0.24034	Reject	p<0.05
ro=0,95	0.959	0.928	0.977	0.28453	Reject	p<0.05
				n=250		
ro=0,0	–0.023	–0.147	0.101	0.03202	Accept	p>0,05
ro=0,1	0.074	–0.051	0.196	0.05561	Accept	p>0,05
ro=0,3	0.199	0.077	0.315	0.0594	Accept	p>0,05
ro=0,5	0.536	0.441	0.619	0.10353	Reject	p<0.05
ro=0,7	0.668	0.593	0.732	0.15862	Reject	p<0.05
ro=0,75	0.728	0.664	0.782	0.17356	Reject	p<0.05
ro=0,80	0.762	0.704	0.809	0.18518	Reject	p<0.05
ro=0,85	0.848	0.809	0.88	0.1922	Reject	p<0.05
ro=0,90	0.924	0.903	0.94	0.22662	Reject	p<0.05
ro=0,95	0.942	0.926	0.954	0.2668	Reject	p<0.05
				n=1,000		
ro=0,0	–0.034	–0.096	0.0228	0.022	Accept	p>0,05
ro=0,1	0.077	0.016	0.139	0.04903	Reject	p<0.05
ro=0,3	0.255	0.196	0.312	0.07695	Reject	p<0.05
ro=0,5	0.467	0.417	0.514	0.11577	Reject	p<0.05
ro=0,7	0.684	0.65	0.716	0.17822	Reject	p<0.05
ro=0,75	0.731	0.7	0.758	0.17669	Reject	p<0.05
ro=0,80	0.81	0.787	0.83	0.18844	Reject	p<0.05
ro=0,85	0.848	0.83	0.865	0.20358	Reject	p<0.05
ro=0,90	0.9	0.888	0.912	0.21422	Reject	p<0.05
ro=0,95	0.954	0.948	0.959	0.2545	Reject	p<0.05

It is seen from Table 3 that for $n = 50$, the independence of the variables is not exactly supported by the uniformity test but for $n = 250$, and $n = 1{,}000$ independency of the variables support gradually by the uniformity test. For $n = 1{,}000$ and $\boldsymbol{\rho} = 0.0$, the correlation test states that variables are independent and Kolmogorov-Smirnov the test states that κ_{n2} is distributed uniformly. On the other hand, for $n = 1{,}000$ where $\boldsymbol{\rho}$ values are greater than 0.0, the dependency characteristic of the original variables produces non-uniform κ_{n2} values.

Example 2

The curvature properties of a bivariate normal surface on real data will be explained in this section. We have been struggling with Covid-19 for more than two years, and there are different studies on this topic. Severe acute respiratory syndrome (SARS) and Covid-19 are compared in terms of similarities and differences in Wilder-Smith et al. (2020). Foldvary (2021) developed a MATLAB tool to analyse and monitor the spread of COVID-19. The author examined the spread based on a geostatistical analysis using MATLAB. A project focused on the spatial correlations among social-demographic, social-demographic, weather information, and atmospheric pollution data with lethality rates and contagion of Covid-19 in Ireland Aghdam–Crowley (2020). The pattern of COVID-19 victims is examined in terms of gender, age, and medical problems. The authors used K-Means and two-step clustering methods for the analysis in Gholipour et al. (2021). The authors studied the effect of Covid-19 on small and medium enterprises in Hungarian Nyikos et al. (2021). In this study, we collect 60-day data on deaths, intubated patients, and daily confirmed virus case numbers given sequentially and regularly between 27 March 2020 and 25 May 2020 from the Covid-19 data of the Turkey Ministry of Health. Many observations of biological processes and characteristics tend to follow a normal distribution. However, the individual case distribution characteristics obtained for this period were observed to have different characteristics than the normal distribution, but using these data: two ratios assumed to be bivariate normally distributed were calculated. The first ratio is the daily death number/case number, and the other is the percentage of the daily intubated patients number/case number. The change of these two ratios is given in Figure 3.

As shown in Figure 3, the Pearson correlation value between the two ratios was obtained as 0.681, and it was observed that there was a moderate, strong linear relationship between them. For the marginal distributions of the two rates considered, the normality test was applied using probability-plot and Kolmogorov-Smirnov test statistics, and the results are shown in Figure A7 in the Appendix.

Figure 3

Pearson correlation and confidence interval between death to case ratio and intubated patients to case ratio (95% CI for Pearson correlation)

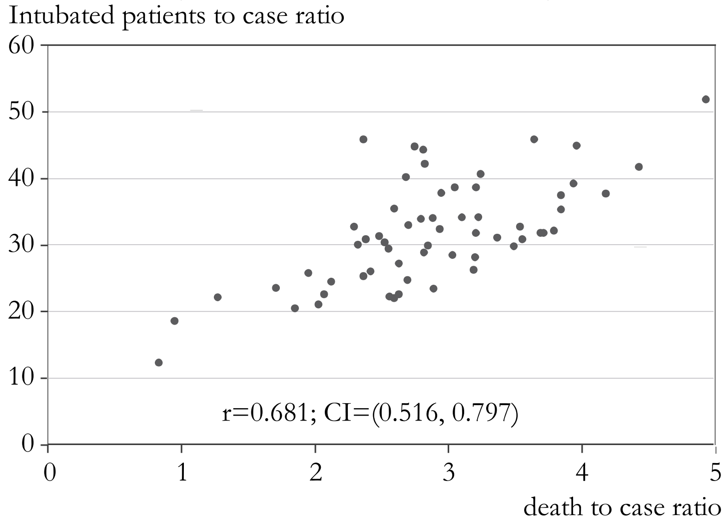

The histograms of both death to case and intubated patients to a) case ratios, b) the normality test for death to case ratio and c) the normality test for intubated patients to case ratio.

Figure A7 in the Appendix shows that the normality assumption is valid for both ratios ($p > 0.15$). The average death to case percentage for the 60-day period was 2.874, and the average for intubated patients to case percentage was 31.57. The covariance structures for the mentioned rates are presented in Table 4.

Table 4

Covariances of ratios

	Death to case ratio	Intubated patients to case ratio
Death to case ratio	0.612343	–
Intubated patients to case ratio	4.259030	63.923556

Within the scope of this study, κ_{n1} and κ_{n2} curvatures are calculated for the Covid-19 mentioned ratios, and are shown in Figure A8 in the Appendix.

The histogram of Gauss and mean curvatures together with κ_{n1} and κ_{n2} are shown in Figure A9 in the Appendix.

As there is a correlation between the examined rates, it is seen from Figure A9 in the Appendix that the uniform distribution structure is disrupted and the right-skewed distribution structure appears for κ_{n1} and the opposite direction skewed distribution character appears for κ_{n2}. In the context of this study, Figure A6 (e) option, which is obtained based on the simulation results for $\boldsymbol{\rho} = 0.70$, is the closest to the correlation value 0.681 which is calculated for the rates. The marginal distributions for κ_{n1} and κ_{n2} calculated according to the Covid-19 ratios that are obtained in this study are given in Figure A10 in the Appendix.

The resulting structure for the marginal curvature distributions and the simulation case for $\boldsymbol{\rho} = 0.7$ are given in Figure A10.

Conclusion

Principal curvatures, Gaussian and mean curvatures at a point on a surface are used for surface characterisation. Statistics is crucial for making some discoveries and predictions using data in many fields. This study presented a novel approach to the bivariate normal distribution and expressed the effectiveness of the correlation of the bivariate normal distribution related to principal curvatures, Gaussian, and mean curvatures of the Bell-shaped surface.

The principal curvatures in the bivariate normal distribution were examined for ten different correlation levels ranging from non-correlated to high correlation. The principal curvature κ_{n1} shows a uniform distribution in the absence of correlation. However, as the correlation increases, it has a left-skewed distribution characteristic. The principal curvature κ_{n2}, unlike the first one, changes from a right-skewed distribution characteristic in the absence of correlation to a left-skewed distribution characteristic as in the first curve when the correlation increases. The change between the principal curvatures is observed in a cubic polynomial model in the absence of correlation. Additionally, the proportional change of the principal curvature κ_{n2} producing negative values for the positive and negative values of the principal curvature κ_{n1} were independent of the correlation characteristics of the bivariate data. The tests show that the bivariate normal distribution surface varies between the concave ellipsoid and hyperboloid structures. The distribution has systematic characteristics arising from the correlation structure at the skirt and top parts of the distribution. Finally, we provided two applications to show the relationship between the independence of the variables and the uniformity of the κ_{n2} values and to present the curvature properties of the bivariate normal surface on the Covid-19 real data. Similarities and differences in the Covid-19 process can be realised between two places according to the principal curvatures.

This study reveals the change between curvature characteristics and variable dependence in bivariate distribution and provides a new perspective on recognising distribution. Hence, the characteristic similarities and differences between two normally distributed bivariate real data can be examined using only the principal curvatures.

Appendix

Figure A1

Contours of the bivariate normal density function

a) Positive correlation

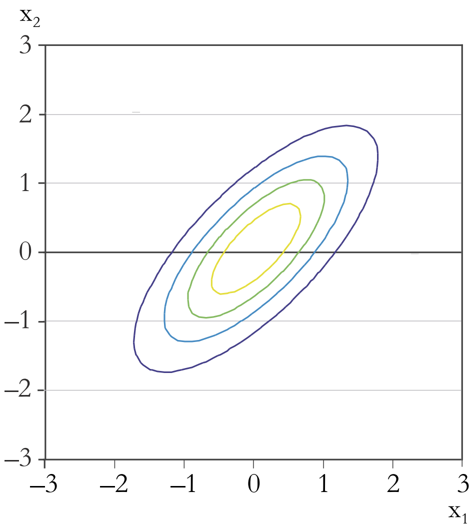

b) Negative correlation

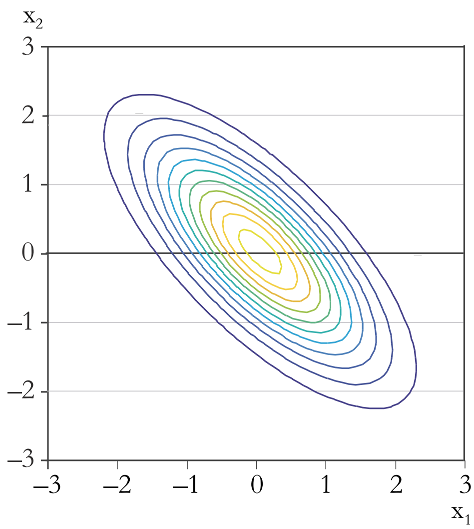

c) Zero correlation

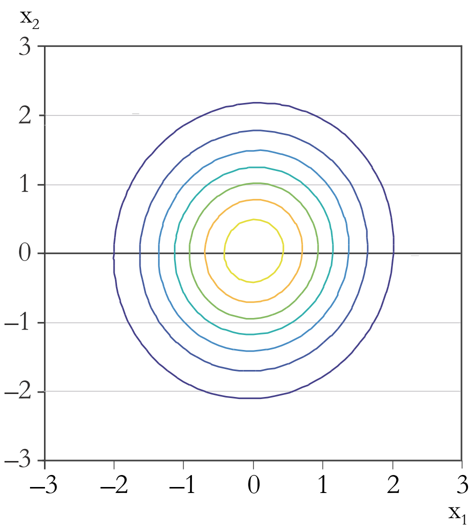

Figure A2

The relationship between the Gauss curvatures of Bell-shaped surface and different values of ρ

a) $\rho = 0.0$

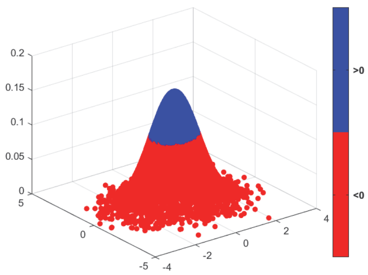

b) $\rho = 0.1$

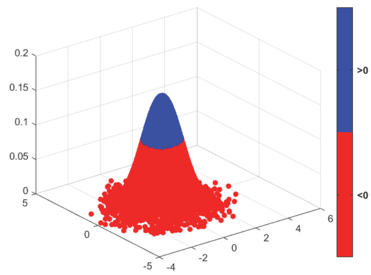

c) $\rho = 0.3$

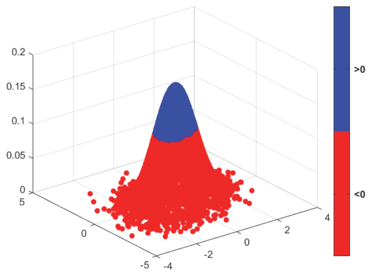

d) $\rho = 0.5$

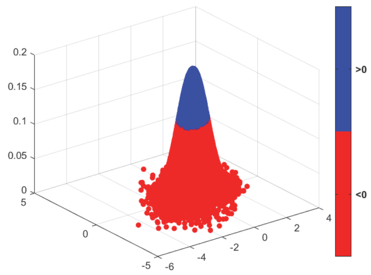

e) $\rho = 0.7$

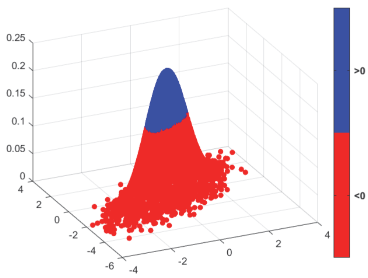

f) $\rho = 0.75$

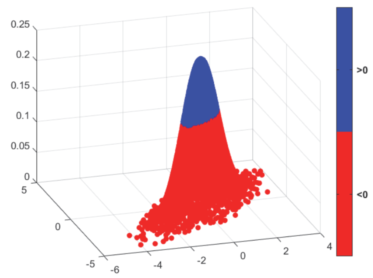

(The figure continued next page.)

(Continued.)

g) $\rho = 0.8$

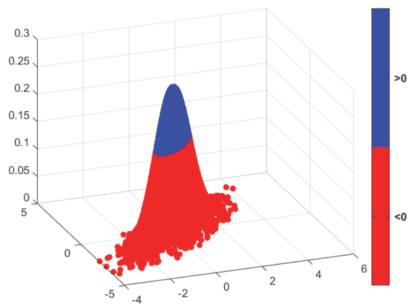

h) $\rho = 0.85$

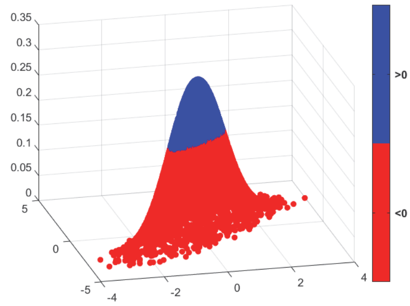

i) $\rho = 0.9$

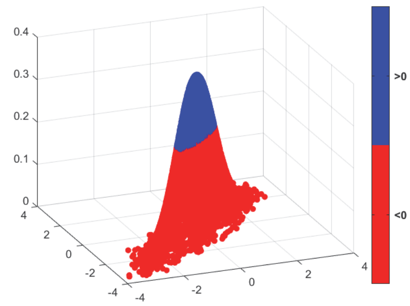

j) $\rho = 0.95$

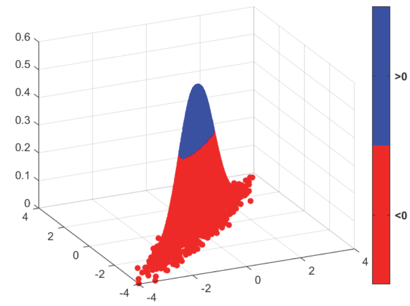

Figure A3

The relationship between the Mean curvatures of
Bell-shaped surface and different values of $\boldsymbol{\rho}$

a) $\boldsymbol{\rho = 0.0}$

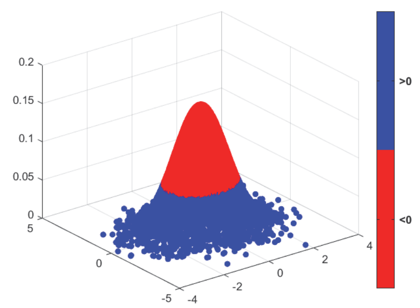

b) $\boldsymbol{\rho = 0.1}$

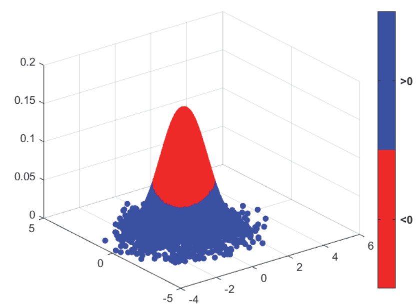

c) $\boldsymbol{\rho = 0.3}$

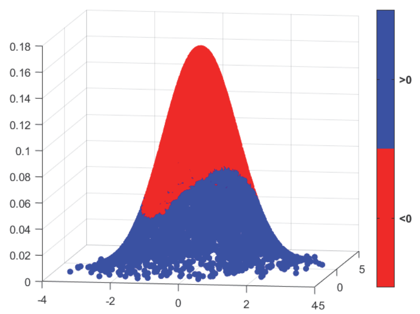

d) $\boldsymbol{\rho = 0.5}$

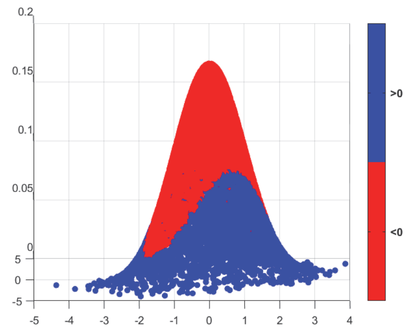

e) $\boldsymbol{\rho = 0.7}$

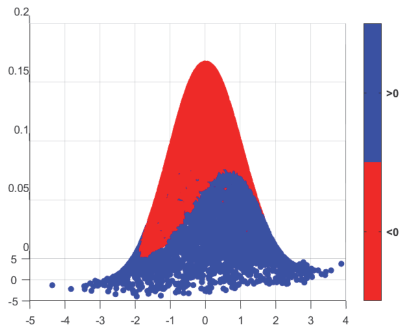

f) $\boldsymbol{\rho = 0.75}$

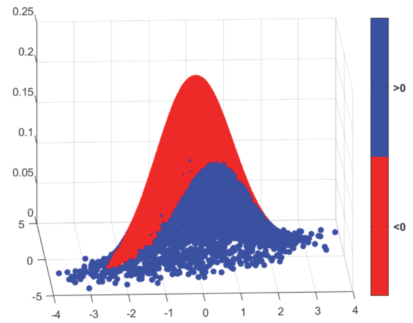

(The figure continued next page.)

(Continued.)

g) $\rho = 0.8$

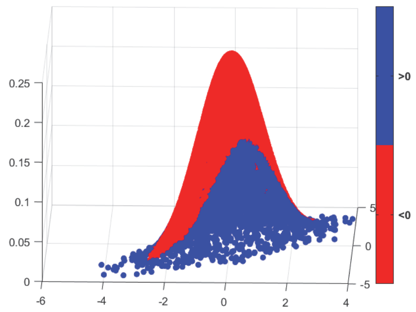

h) $\rho = 0.85$

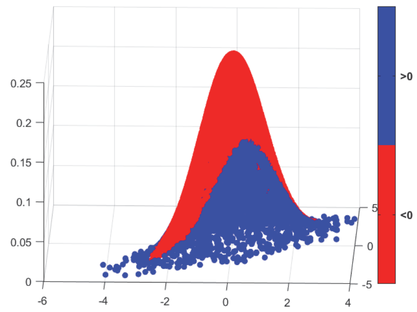

i) $\rho = 0.9$

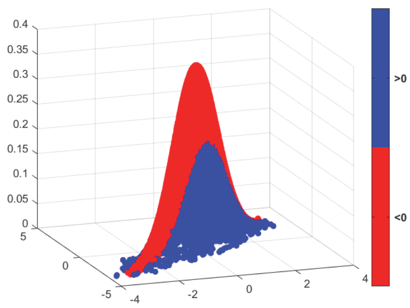

j) $\rho = 0.95$

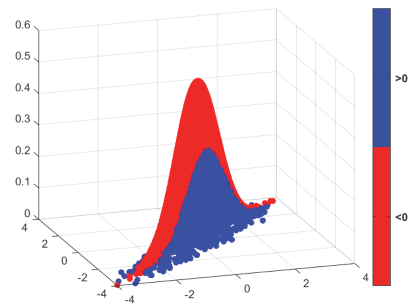

Figure A4

The distribution of the values of κ_{n1} for the values of ρ

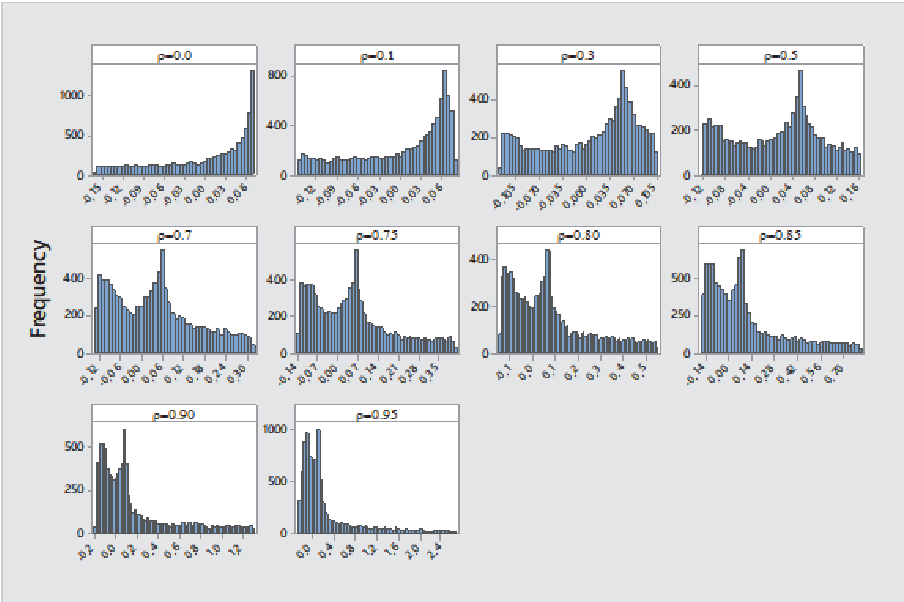

Figure A5

The distribution of the values of κ_{n2} for the values of ρ

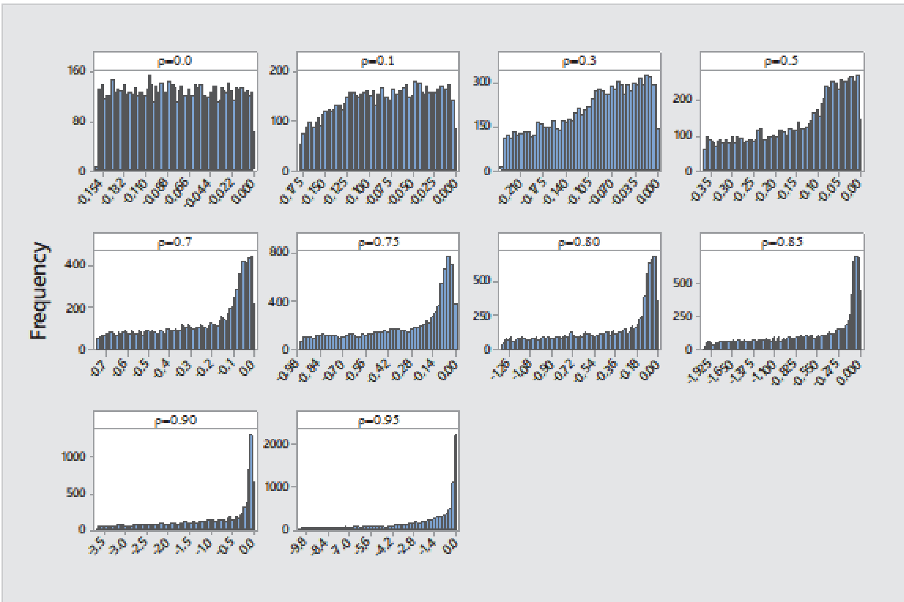

Figure A6

The relationship between the principal curvatures

κ_{n1} and κ_{n2} for different values of ρ

a)

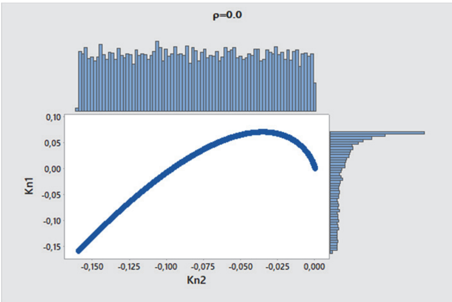

b)

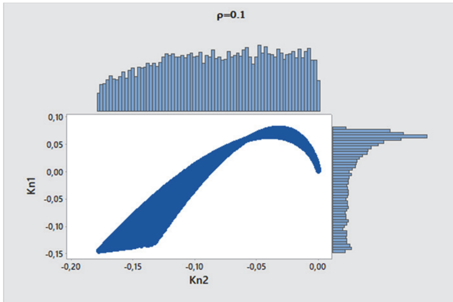

c)

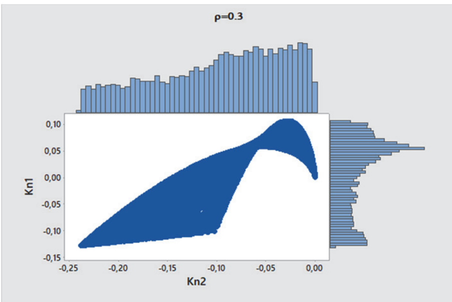

d)

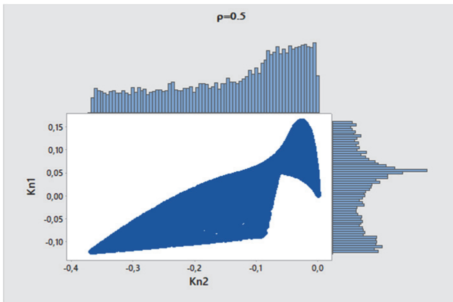

e)

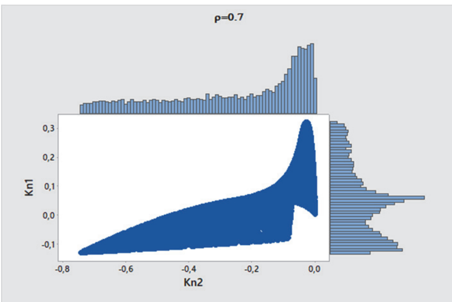

f)

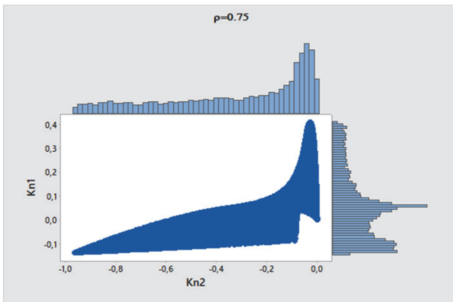

(The figure continued next page.)

(Continued.)

g)

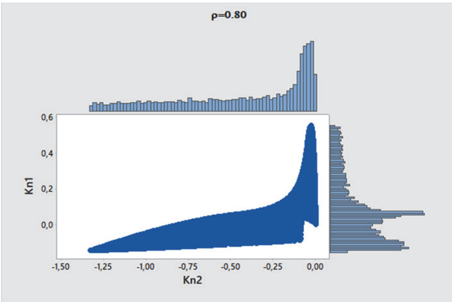

h)

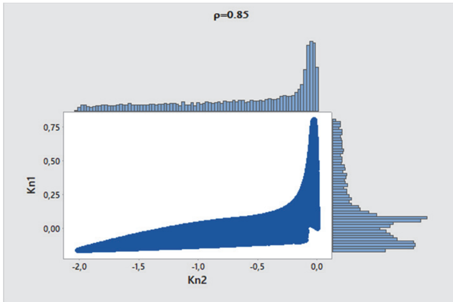

i)

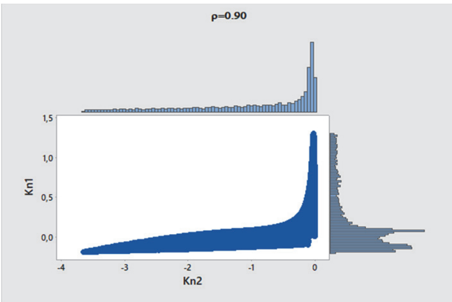

j)

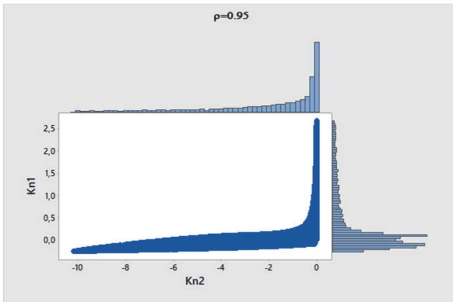

Figure A7

The histograms and normality test for both death to case and intubated patients to case ratios

a) Case ratios

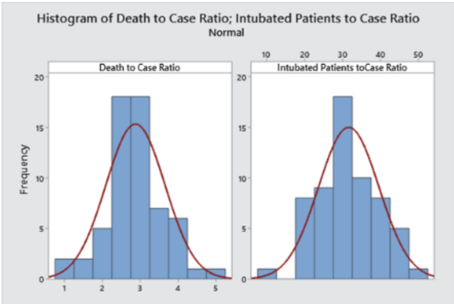

b) The normality test for death to case ratio

c) The normality test for intubated patients to case ratio

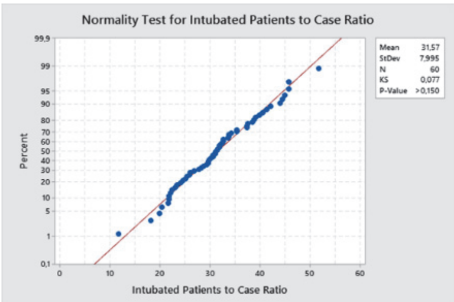

Figure A8

κ_{n1} and κ_{n2} curvatures of the ratios that are death to case and intubated patients to case

a) κ_{n1}curvature of the ratios b). κ_{n2} curvature of the ratios

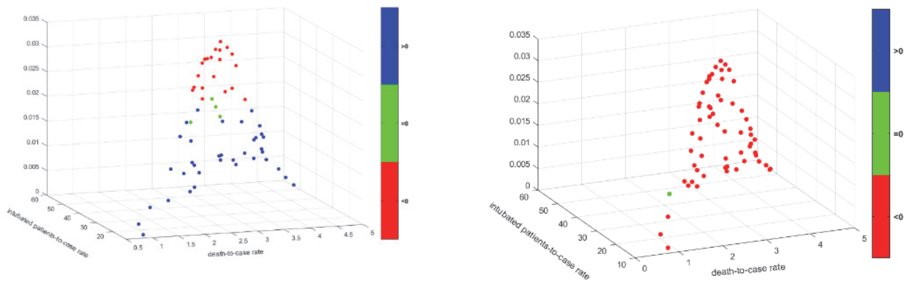

Figure A9

The histogram of Gauss and mean curvatures together with the principal curvatures κ_{n1} and κ_{n2}

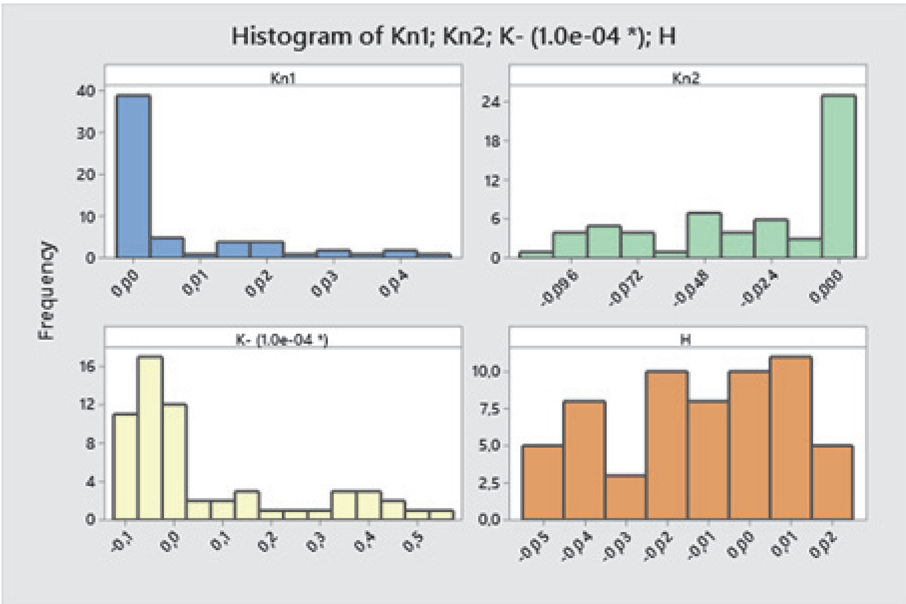

Figure A10

The histogram of Gauss and mean curvatures together with the principal curvatures κ_{n1} and κ_{n2}

a) The marginal distributions of κ_{n1} and κ_{n2}

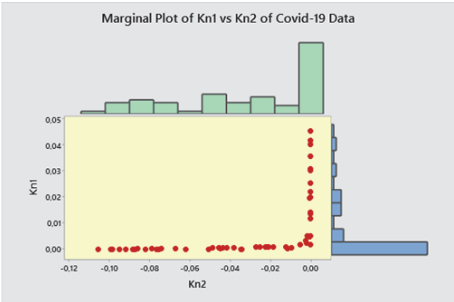

b) The relationship between κ_{n1} and κ_{n2} for ρ = 0.7

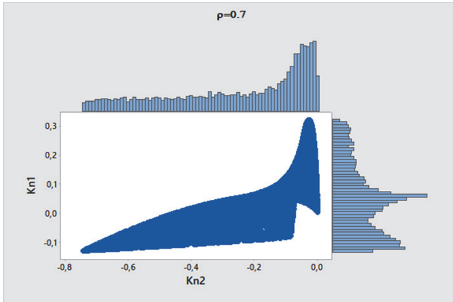

REFERENCES

AGHDAM, M.–CROWLEY, Q. (2020): *Modeling of the covid-19 epidemic using geostatistical methods and based on the investigation of spatial correlations between atmospheric pollution, meteorological factors, age, sex, health condition, and lockdown phases with levels of virus contagion and lethality* Technical Report, CEU. https://doi.org/10.5281/zenodo.4393072

ARELLANO-VALLE, R. B.–GENTON, M. G. (2010): Multivariate unified skew-elliptical distributions *Chilean Journal of Statistics* 1 (1): 17–33.

AZZALINI, A. (1985): A class of distributions which includes the normal ones *Scandinavian Journal of Statistics* 12 (2): 171–178.

AZZALINI, A.–CHIOGNA, M. (2004): Some results on the stress–strength model for skew-normal variates *Metron - International Journal of Statistics* 62 (3): 315–326.

BEDI, S.–GRAVELLE, S.–CHEN, Y. H. (1997): Principal curvature alignment technique for machining complex surfaces *Journal of Manufacturing Science and Engineering* 119 (4B): 756–765. https://doi.org/10.1115/1.2836821

BRANCO, M. D.–DEY, D. K. (2001): A general class of multivariate skew elliptical distributions *Journal of Multivariate Analysis* 79 (1): 99–113. https://doi.org/10.1006/jmva.2000.1960

CHEN, J. H.–HUNG, W. L. (2019): Parametrizing the Kepler exoplanet period- radius distribution with the bivariate normal inverse Gaussian distribution *Journal of Applied Statistics* 46 (4): 725–736. https://doi.org/10.1080/02664763.2018.1508558

DENG, H.–ZHANG, W.–MORTENSEN, E.–DIETTERICH, T.–SHAPIRO, L. (2007): Principal curvature-based region detector for object recognition *2007 IEEE Conference on Computer Vision and Pattern Recognition, 2007* pp. 1–8. https://doi.org/10.1109/CVPR.2007.382972

DILL, J. (1981): An application of color graphics to the display of surface curvature *ACM SIGGRAPH Computer Graphics* 15 (3): 153–161. https://doi.org/10.1145/965161.806801

FLORO, J. A.–CHASON, E. (2001): Curvature based techniques for real time stress measurement during thin film growth. In: AUCIELLO, O.–KRAUSS, A. R. (eds.): *In Situ and Real Time Characterization of Thin Films* pp. 191–216., Wiley, New York.

FOLDVARY, L. (2021): Geostatistical investigations on the spread of Covid-19 *International Journal of Geoinformatics* 17 (1): 75–84. https://doi.org/10.52939/ijg.v17i1.1713

GHOLIPOUR, E.–VIZVARI, B.–BABAQI, T.–TAKACS, S. (2021): Statistical analysis of the Hungarian covid-19 victims *Journal of Medical Virology* 93 (12): 6660–6670. https://doi.org/10.1002/jmv.27242

HENZE, N. A. (1986): A probabilistic representation of the skew-normal distribution *Scandinavian Journal of Statistics* 13 (4): 271–275.

HOLTMANN-RICE, D.–KUNSBERG, B.–ZUCKER, S. (2018): Tensors, differential geometry and statistical shading analysis *Journal of Mathematical Imaging and Vision* 60: 968–992. https://doi.org/10.1007/s10851-018-0815-z

JAFARI, A. A.–ROOZGAR, R.–KUNDU, D. (2018): On bivariate generalized exponential power series class of distributions *Journal of Iranian Statistical Society* 17 (1): 63–88. https://doi.org/10.29252/jirss.17.1.63

JAMALIZADEH, A.–BALAKRISHNAN, N. (2019): Conditional distributions of multi- variate normal mean–variance mixtures *Statistics and Probability Letters* 145: 312–316. https://doi.org/10.1016/j.spl.2018.10.005

KRSEK, P.–LUKACS, G.–MARTIN, R. R. (1998): Algorithms for computing curvatures from range data. In*:* CRIPPS, R.: *The Mathematics of Surfaces VIII* pp. 1–16*.,* Information Geometers.

KUNDU, D.–GUPTA, A. (2014): On bivariate weibull-geometric distribution *Journal of Multivariate Analysis* 123: 19–29. https://doi.org/10.1016/j.jmva.2013.08.004

LEV, J.–LIM, J. H.–OUARTI, N. (2017): Principal curvature of point cloud for 3d shape recognition *2017 IEEE International Conference on Image Processing (ICIP)* pp. 610–614. https://doi.org/10.1109/ICIP.2017.8296353

MAHMOUDI, E.–MAHMOODIAN, H. (2017): A new bivariate distribution obtained by compounding the bivariate normal and geometric distributions *Journal of Statistical Theory and Applications* 16 (2): 198–208. https://doi.org/10.2991/jsta.2017.16.2.5

NYIKOS, G.–SOHA, B.–BERES, A. (2021): Entrepreneurial resilience and firm performance during the covid-19 crisis evidence from Hungary *Regional Statistics* 11 (3): 29–59. https://doi.org/10.15196/RS110307

OMAIR, M.–ALMUHAYFITH, F.–ALZAID, A. (2018): A bivariate model based on com- pound negative binomial distribution *Revista Colombiana de Estadistica* 41 (1): 87–108. http://dx.doi.org/10.15446/rce.v41n1.57803

PRESSLEY, A. N. (2010): *Elementary Differential Geometry* Springer-Verlag, London.

ROOZEGAR, R.–JAFARI, A. A. (2017): On bivariate generalized linear failure rate- power series class of distributions *Iranian Journal of Science and Technology, Transactions A: Science* 41 (3): 693–706.

SBOUI, I.–JRIBI, M.–GHORBEL, F. (2017): 3d human shapes correspondence using the principal curvature fields on a local surface parametrization In: *Proceedings of The 12th International Joint Conference on Computer Vision, Imaging and Computer Graphics Theory and Applications (Visigrapp 2017)* Volume 4, pp. 631–636., Porto.

SHIMAMOTO, K. (2019): Empirical analysis of the distribution of urban parks in Japan *Regional Statistics* 9 (2): 148–172. https://doi.org/10.15196/RS090203

TANAKA, H. T.–IKEDA, M.–CHIAKI, H. (1998): Curvature-based face surface recognition using spherical correlation. principal directions for curved object recognition. In: *Proceedings Third IEEE International Conference on Automatic Face and Gesture Recognition* pp. 372–377. https://doi.org/10.1109/AFGR.1998.670977

THEIL, S. L. (1984): A Riemannian geometry of the multivariate normal model *Scandinavian Journal of Statistics* 11 (4): 211–223.

TREMBLAY-DARVEAU, C.–SHEERAN, P. S.–VU, C. K.–WILLIAMS, R.–BRUCE, M.–BURNS, P. N. (2018): 3-d perfusion imaging using principal curvature detection rendering *IEEE Transactions on Ultrasonics, Ferroelectrics, and Frequency Control* 65 (12): 2286–2295. https://doi.org/10.1109/TUFFC.2018.2854727

VEMURI, B. C.–MITICHE, A.–AGGARWAL, J. K. (1986): Curvature based representation of objects from range data *Image and Vision Computing* 4 (2): 107–114. https://doi.org/10.1016/0262-8856(86)90029-6

WANG, F.–YOU, H. J.–QIU, X. L.–YAO, X. H. (2018): Shape similarity measure method based on principal curvature enhancement distance transformation *Journal of Infrared and Millimeter Waves* 37 (1): 72–80. https://doi.org/10.11972/j.issn.1001-9014.2018.01.014

WILDER-SMITH, A.–CHIEW, C. J.–VERNON, J. L. (2020): Can we contain the COVID-19 outbreak with the same measures as for SARS? *The Landset* 20 (5): e102-e107. https://doi.org/10.1016/S1473-3099(20)30129-8